Biomedical Optics EXPRESS

Optimizing modulation frequency for structured illumination in a fiber-optic microendoscope to image nuclear morphometry in columnar epithelium

P. A. Keahey,[1,*] T. S. Tkaczyk,[1] K. M. Schmeler,[2] and R. R. Richards-Kortum[1]

[1]*Department of Bioengineering, Rice University, 6100 Main Street, Houston, Texas 77025 USA*
[2]*Department of Gynecologic Oncology and Reproductive Medicine, The University of Texas MD Anderson Cancer Center, 1100 Holcombe Boulevard, Houston, TX 77030 USA*
**pelham.keahey@rice.edu*

Abstract: Fiber-optic microendoscopes have shown promise to image the changes in nuclear morphometry that accompany the development of precancerous lesions in tissue with squamous epithelium such as in the oral mucosa and cervix. However, fiber-optic microendoscopy image contrast is limited by out-of-focus light generated by scattering within tissue. The scattering coefficient of tissues with columnar epithelium can be greater than that of squamous epithelium resulting in decreased image quality. To address this challenge, we present a small and portable microendoscope system capable of performing optical sectioning using structured illumination (SI) in real-time. Several optical phantoms were developed and used to quantify the sectioning capabilities of the system. Columnar epithelium from cervical tissue specimens was then imaged *ex vivo*, and we demonstrate that the addition of SI achieves higher image contrast, enabling visualization of nuclear morphology.

OCIS codes: (170.0170) Medical optics and biotechnology; (060.2350) Fiber optics imaging; (170.1610) Clinical applications; (170.2150) Endoscopic imaging; (170.2520) Fluorescence microscopy; (170.6935) Tissue characterization.

References and links

1. J. Ferlay, I. Soerjomataram, M. Ervik, R. Dikshit, S. Eser, C. Mathers, M. Rebelo, D. M. Parkin, D. Forman, and F. Bray, "GLOBOCAN 2012 v1.0, Cancer Incidence and Mortality Worldwide: IARC CancerBase No. 11," Lyon, France: International Agency for Research on Cancer; 2013. Available from: http://globocan.iarc.fr, accessed on October 9th, 2014.
2. World Health Organization, *Guidelines for screening and treatment of precancerous lesions for cervical cancer prevention* (WHO Guidelines, 2013).
3. T. J. Muldoon, M. C. Pierce, D. L. Nida, M. D. Williams, A. Gillenwater, and R. Richards-Kortum, "Subcellular-resolution molecular imaging within living tissue by fiber microendoscopy," Opt. Express **15**(25), 16413–16423 (2007).
4. D. Shin, M. C. Pierce, A. M. Gillenwater, M. D. Williams, and R. R. Richards-Kortum, "A Fiber-Optic Fluorescence Microscope Using a Consumer-Grade Digital Camera for in Vivo Cellular Imaging," PLoS ONE **5**(6), e11218 (2010).
5. D. Shin, M. A. Protano, A. D. Polydorides, S. M. Dawsey, M. C. Pierce, M. K. Kim, R. A. Schwarz, T. Quang, N. Parikh, M. S. Bhutani, F. Zhang, G. Wang, L. Xue, X. Wang, H. Xu, S. Anandasabapathy, and R. R. Richards-Kortum, "Quantitative Analysis of High-Resolution Microendoscopic Images for Diagnosis of Esophageal Squamous Cell Carcinoma," Clin. Gastroenterol. Hepatol. **13**(2), 272–279 (2015).
6. N. D. Parikh, D. Perl, M. H. Lee, B. Shah, Y. Young, S. S. Chang, R. Shukla, A. D. Polydorides, E. Moshier, J. Godbold, E. Zhou, J. Mitcham, R. Richards-Kortum, and S. Anandasabapathy, "In vivo diagnostic accuracy of high-resolution microendoscopy in differentiating neoplastic from non-neoplastic colorectal polyps: a prospective study," Am. J. Gastroenterol. **109**(1), 68–75 (2014).
7. S. S. Chang, R. Shukla, A. D. Polydorides, P. M. Vila, M. Lee, H. Han, P. Kedia, J. Lewis, S. Gonzalez, M. K. Kim, N. Harpaz, J. Godbold, R. Richards-Kortum, and S. Anandasabapathy, "High resolution microendoscopy for classification of colorectal polyps," Endoscopy **45**(7), 553–559 (2013).

#232001 - $15.00 USD Received 7 Jan 2015; revised 9 Feb 2015; accepted 14 Feb 2015; published 19 Feb 2015

8. P. M. Vila, M. J. Kingsley, A. D. Polydorides, M. A. Protano, M. C. Pierce, J. Sauk, M. K. Kim, K. Patel, J. H. Godbold, J. D. Waye, R. Richards-Kortum, and S. Anandasabapathy, "Accuracy and interrater reliability for the diagnosis of Barrett's neoplasia among users of a novel, portable high-resolution microendoscope," Dis. Esophagus **27**(1), 55–62 (2014).
9. M. K. Quinn, T. C. Bubi, M. C. Pierce, M. K. Kayembe, D. Ramogola-Masire, and R. Richards-Kortum, "High-resolution microendoscopy for the detection of cervical neoplasia in low-resource settings," PLoS ONE **7**(9), e44924 (2012).
10. T. J. Muldoon, S. Anandasabapathy, D. Maru, and R. Richards-Kortum, "High-resolution imaging in Barrett's esophagus: a novel, low-cost endoscopic microscope," Gastrointest. Endosc. **68**(4), 737–744 (2008).
11. R. Regunathan, J. Woo, M. C. Pierce, A. D. Polydorides, M. Raoufi, S. Roayaie, M. Schwartz, D. Labow, D. Shin, R. Suzuki, M. S. Bhutani, L. G. Coghlan, R. Richards-Kortum, S. Anandasabapathy, and M. K. Kim, "Feasibility and preliminary accuracy of high-resolution imaging of the liver and pancreas using FNA compatible microendoscopy (with video)," Gastrointest. Endosc. **76**(2), 293–300 (2012).
12. T. J. Muldoon, PhD, D. Roblyer, PhD, M. D. Williams, MD,V. M. T. Stepanek, MD, PhD, R. Richards-Kortum, PhD, and A. M. Gillenwater, MD, "Noninvasive imaging of oral neoplasia with a high-resolution fiber-optic microendoscope," Head Neck **34**(3), 305–312 (2010).
13. I. Georgakoudi, E. E. Sheets, M. G. Müller, V. Backman, C. P. Crum, K. Badizadegan, R. R. Dasari, and M. S. Feld, "Trimodal spectroscopy for the detection and characterization of cervical precancers in vivo," Am. J. Obstet. Gynecol. **186**(3), 374–382 (2002).
14. C. Redden Weber, R. A. Schwarz, E. N. Atkinson, D. D. Cox, C. Macaulay, M. Follen, and R. Richards-Kortum, "Model-based analysis of reflectance and fluorescence spectra for in vivo detection of cervical dysplasia and cancer," J. Biomed. Opt. **13**(6), 064016 (2008).
15. M. H. Koucky and M. C. Pierce, "Axial response of high-resolution microendoscopy in scattering media," Biomed. Opt. Express **4**(10), 2247–2256 (2013).
16. N. Bozinovic, C. Ventalon, T. Ford, and J. Mertz, "Fluorescence endomicroscopy with structured illumination," Opt. Express **16**(11), 8016–8025 (2008).
17. M. A. A. Neil, R. Juskaitis, and T. Wilson, "Method of obtaining optical sectioning by using structured light in a conventional microscope," Opt. Lett. **22**(24), 1905–1907 (1997).
18. T. Wilson, "Optical sectioning in fluorescence microscopy," J. Microsc. **242**(2), 111–116 (2011).
19. M. Kyrish, J. Dobbs, S. Jain, X. Wang, D. Yu, R. Richards-Kortum, and T. S. Tkaczyk, "Needle-based fluorescence endomicroscopy via structured illumination with a plastic, achromatic objective," J. Biomed. Opt. **18**(9), 096003 (2013).
20. D. Xu, T. Jiang, A. Li, B. Hu, Z. Feng, H. Gong, S. Zeng, and Q. Luo, "Fast optical sectioning obtained by structured illumination microscopy using a digital mirror device," J. Biomed. Opt. **18**(6), 060503 (2013).
21. A. G. York, S. H. Parekh, D. Dalle Nogare, R. S. Fischer, K. Temprine, M. Mione, A. B. Chitnis, C. A. Combs, and H. Shroff, "Resolution doubling in live, multicellular organisms via multifocal structured illumination microscopy," Nat. Methods **9**(7), 749–754 (2012).

1. Introduction

Cervical cancer is responsible for the death of 266,000 women worldwide each year, with 87% of these deaths occurring in low and middle incomes countries (LMICs). Cervical cancer is the second most common cancer in women living in low income regions and the third most deadly [1]. The Papanicolaou test with follow-up colposcopy and histology via biopsy has proven to be an effective early screening technique which has drastically reduced cervical cancer incidence in well-developed regions. However, these screening methods have not been implemented widely in LMICs due to high cost and lack of infrastructure and expertise [2]. There is a need for an imaging procedure which can rapidly and non-invasively screen cervical tissue *in vivo* and provide clinicians with the necessary histological information to identify pre-cancerous lesions in real-time allowing for immediate treatment to prevent the development of invasive disease.

We previously reported a high resolution microendoscope (HRME). The HRME can provide sub-cellular resolution images of tissue *in vivo* comparable to histological slides from biopsies normally examined by pathologists using bench-top microscopes to diagnose pre-cancer [3]. The HRME uses a flexible fiber-optic probe to perform epifluorescent sub-cellular resolution imaging of tissue placed in contact with the tip of the bundle and has a depth of focus of approximately 20 μm [4]. Proflavine, a contrast agent which highlights the nuclei of cells, is commonly used in conjunction with the HRME to assess nuclear morphology. The low cost, portability, and real-time imaging capabilities of the HRME have enabled a number of *ex vivo* and *in vivo* trials to evaluate the ability of the HRME to identify early neoplastic

#232001 - $15.00 USD Received 7 Jan 2015; revised 9 Feb 2015; accepted 14 Feb 2015; published 19 Feb 2015

lesions. These studies were conducted on regions of tissue containing squamous epithelium and columnar epithelium [5–12]. Squamous epithelium is flat and has a relatively low optical scattering coefficient compared to columnar epithelium [13, 14]. HRME images of normal squamous epithelium can be easily evaluated to assess characteristics such as nuclear to cytoplasm ratio and nuclear size, which have been shown to be indicative of dysplasia in squamous epithelium [5]. In contrast, the optical scattering coefficient of columnar epithelium is higher and the surface is invaginated [14]. This increased scattering can lead to increased out-of-focus light in HRME images, thereby reducing contrast between nuclei in the focal plane (tissue surface) and background.

The cervix contains both squamous and columnar epithelium with neoplastic lesions usually developing at the junction of the two tissue types. Therefore, imaging cervical tissue requires a device which can image nuclear morphometry in both types of epithelium. Unfortunately, images of columnar epithelium in the cervix obtained using the existing HRME often lack sufficient contrast to visualize nuclear morphometry. The fiber-bundle does not provide any inherent optical sectioning capabilities to the HRME [15].

Structured illumination (SI) imaging has been demonstrated as a means to perform optical sectioning through a fiber-bundle as described by Bozinovic et al. [16]. Structured illumination imaging works by modulating the illumination pathway with a moveable grid pattern which is imaged onto the proximal end of a fiber-bundle. Three images are captured in sequence with the grating translated by one-third the period in each. Images are then recombined computationally as described by Neil et al. [17]. The resulting combined image provides out-of-focus light rejection similar in strength to confocal microscopy. Furthermore, SI sectioning strength can be adjusted based on the modulation frequency. A higher frequency increases axial sectioning, but in practice also diminishes contrast between the grid image and the sample. This loss is largely due to the optical transfer function of the grating and sampling by the fiber-bundle. This reduction in grating contrast can cause in-focus signal loss thereby reducing the dynamic range [16, 18].

Kyrish et al. developed a table-top device which successfully implemented SI imaging through a flexible fiber-bundle [19]. This system was capable of imaging tissue using SI, but it was restricted to an optical breadboard and lacked the portability the HRME afforded clinicians for use in the clinic or operating room. The work also only focused on imaging with a single modulation frequency.

Building upon this work, here we present a portable Structured Illumination-HRME (SI-HRME) which is capable of performing SI imaging in real-time. We quantified the axial response of the SI-HRME by analyzing the imaging performance at different modulation frequencies in several optical phantoms designed to model feature sizes expected to be found in tissue. A pre-clinical study was then performed using samples of columnar epithelium on cervical tissue samples. Tissue was examined *ex vivo* to assess contrast improvements with the addition of SI and to determine whether there is an optimal modulation frequency (amount of sectioning) for revealing nuclear morphometry in cervical columnar epithelium.

2. Methods and materials

2.1 SI-HRME system and assembly

Figure 1 presents the optical diagram for the SI-HRME and a photograph of the device that was used in this study. A high power LED (Ledengine, LZ1-10DB00) emits 455 nm light which passes through an excitation filter (Chroma ET470/40x) and is collimated by a collection lens relay (Thorlabs, AC254-050-A & AC254-030-A). This illuminates a 5 lpm, 10 lpm or 20 lpm Ronchi grating (Edmund Optics, 57-903, 38-258, 57-885). These gratings are mounted on a two-axis stepper motor system (Zaber, T-LS28M & LSA10A-T4) used to step the Ronchi grating laterally for SI imaging and to move the grating out-of-focus for quick transition to standard HRME (HRME without SI) imaging for comparison. The mounted

#232001 - $15.00 USD Received 7 Jan 2015; revised 9 Feb 2015; accepted 14 Feb 2015; published 19 Feb 2015

grating is then imaged via the condenser lens (Thorlabs, AC254-035-A) onto the rear of the objective (Olympus RMS10X) after reflecting off a dichroic mirror (Chroma, 475DCXRU). A fiber-optic bundle (Myriad Fiber Imaging, FIGH-30-850N) with 790 µm imaging diameter comprised of 30,000 individual fibers is placed at the objective's working distance. The fiber-bundle relays the modulated excitation to the sample, and the corresponding modulated emission returns via the same fiber. Emission is focused onto a monochromatic CCD (Point Grey, GS2-GE-20S4M-C) by a tube lens (Thorlabs, AC254-100-A), shown in Fig. 1(a).

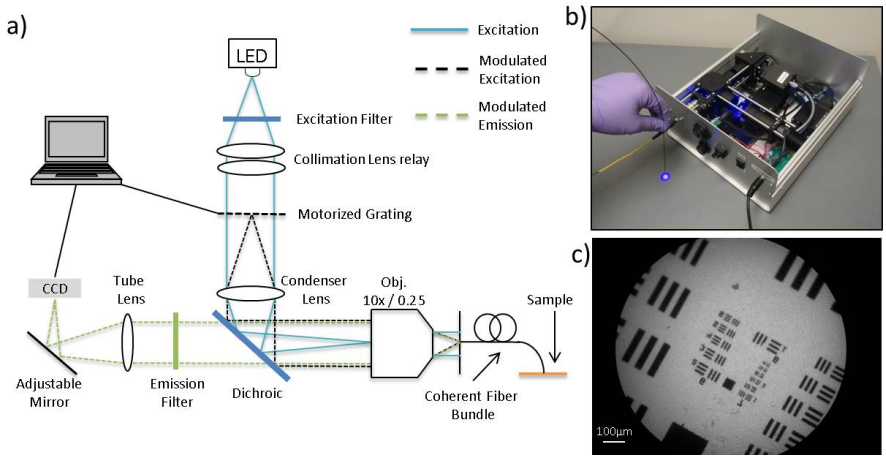

Fig. 1. Schematic diagram of the SI-HRME system **(a)**. Photo of the SI-HRME with lid removed and hand held fiber-bundle probe **(b)**. Image of a standard air force resolution target. Group 6 element 6 is resolvable corresponding to ~4.4µm lateral spatial resolution **(c)**.

Structured illumination imaging is performed by acquiring three images sequentially with the grating stepped laterally by one-third the period by the stepper motor. The images are then combined computationally and displayed in real-time. The SI-HRME acquires images at 11 fps in standard HRME mode. SI imaging requires three images to be combined to form one sectioned image for an effective frame rate of 11/3 (3.67) fps. Camera and motor synchronization along with all real-time image processing was performed by a custom Labview VI (National Instruments). The blue illumination LED is controlled by a PCB mounted LED driver (Luxeon, 3021-D-E-1000). The device is housed within a 134.5 x 261 x 300 mm aluminum case (Newark, M5504110).

2.2 Optical phantoms

Optical phantoms were developed and imaged similarly to the methods described by Koucky et al., but with modifications to the imaging process to evaluate the sectioning capabilities of the SI-HRME [15]. The 2D phantom was developed by pipetting 25 µL of 15 µm fluorescent polystyrene microspheres (Life Technologies, F-21010) in solution onto a clear glass slide. The slide was allowed to dry at room temperature for twenty minutes before imaging began. The 3D non-scattering phantom was prepared by mixing 1 mL of microspheres with 9 mL of DI H_2O and 0.1 g of agar (Sigma A9799). The sample was then vortexed until the contents were evenly distributed. The sample tube was then placed in a boiling water bath and allowed to heat for 10 minutes to melt the agar for proper mixing. The sample was then removed and vortexed a second time before being poured into a 60 mm petri dish and allowed to cool at room temperature for several hours. The 3D scattering phantom was prepared by mixing 1 mL of microspheres with 8 mL of DI H_2O, 1 mL intralipid (Sigma I141), and 0.1 g of agar. The same procedure was then followed that was used to make the non-scattering phantom. The scattering coefficient for the 3D phantom was found to be 7.52 cm^{-1} which approximates the measured scattering coefficient of cervical columnar tissue [14].

#232001 - $15.00 USD Received 7 Jan 2015; revised 9 Feb 2015; accepted 14 Feb 2015; published 19 Feb 2015

2.3 Imaging the phantoms

The 2D imaging phantom glass slide was mounted to a stepper motor (Zaber, LSA10A-T4), and the fiber-bundle was placed in contact with the glass slide. The glass slide was then stepped away in 20 μm increments and images were captured at each location. The Ronchi grating mounted within the SI-HRME was manually exchanged and the process repeated for the same field-of-view (FOV). Variable modulation frequencies were achieved by placing three different Ronchi gratings in the illumination pathway: 5 lpm, 10 lpm, and 20 lpm. The condenser lens and objective demagnified the grating and each grating corresponded to 10.1 lpm, 20.3 lpm, and 40.5 lpm respectively in the image plane. Standard HMRE images (structured illumination off) were acquired by simply moving the grating out of the focal plane of the condenser lens via the stepper motor. The average intensity of each image was measured using ImageJ software (NIH ver 1.47v).

The 3D agar phantoms were imaged by placing the fiber-bundle in gentle contact with the gel's surface. Images were again acquired with the SI-HRME with and without SI for each of the modulation frequencies. Camera gain was set to 0 dB, exposure 3.0 ms. Neither the agar gel nor the fiber-bundle were moved during 3D phantom imaging. Areas imaged were then marked to locate the same field-of-view later, but not in a way to impede imaging. The gels were then transferred to a Zeiss microscope (Zeiss, Imager Z.1), and the same FOVs imaged by the SI-HRME were found. The surface of the gel was considered $z = 0$ μm, and the depth of each microsphere was found by translating the vertical stage into the working distance of a 20x objective (Zeiss, Plan-Apochromat 20x/0.8). Sphere depth was recorded in reference to the surface of the gel. Average individual sphere intensity was measured by manually circling an ROI for each sphere in ImageJ.

2.4 Ex vivo tissue samples

Cervical tissue samples were collected from patients who had undergone a loop electrosurgical excision procedure for cervical dysplasia. Patients gave informed consent and the study was reviewed and approved by the IRBs at Rice University and University of Texas MD Anderson Cancer Center. Proflavine (0.01% w/v in sterile PBS) was topically applied to each tissue specimen and then imaged immediately. Camera exposure was approximately 30 ms, but was adjusted slightly dependent on site-to-site variation in fluorescent intensity as to avoid saturation. Gain was set to 0 dB. The fiber-optic bundle was placed in light contact with the epithelial surface and scanned across the squamous-columnar junction. The average nuclear to background intensity ratio (NBR) was calculated by manually segmenting nuclear regions and areas outside nuclei (cytoplasm) of the imaged sites using ImageJ. The intensity of each nuclear and background ROI was found and averaged respectively. The NBR was used as a method of contrast comparison between modulation frequencies.

3. Results

3.1 2D phantom imaging

Figure 2 shows SI-HRME images of the 15 μm microspheres deposited as a monolayer on the surface of the glass slide as a function of the distance away from the tip of the fiber-bundle. Figures 2(a)-2(d) shows the same FOV for different modulation frequencies when the glass slide is resting against the fiber-bundle. As the modulation frequency increases, there is a visible decrease in average intensity. Figures 2(e)-2(h) shows the same FOV when the glass slide is 60 μm from the fiber-bundle and sphere diameter has visibly increased due to defocus. Microspheres in the no SI image are still quite visible, but are progressively attenuated as modulation frequency increases. Brightness was increased equally in all images to enhance visibility of dimmer spheres. All quantification occurred prior to any adjustment.

#232001 - $15.00 USD Received 7 Jan 2015; revised 9 Feb 2015; accepted 14 Feb 2015; published 19 Feb 2015

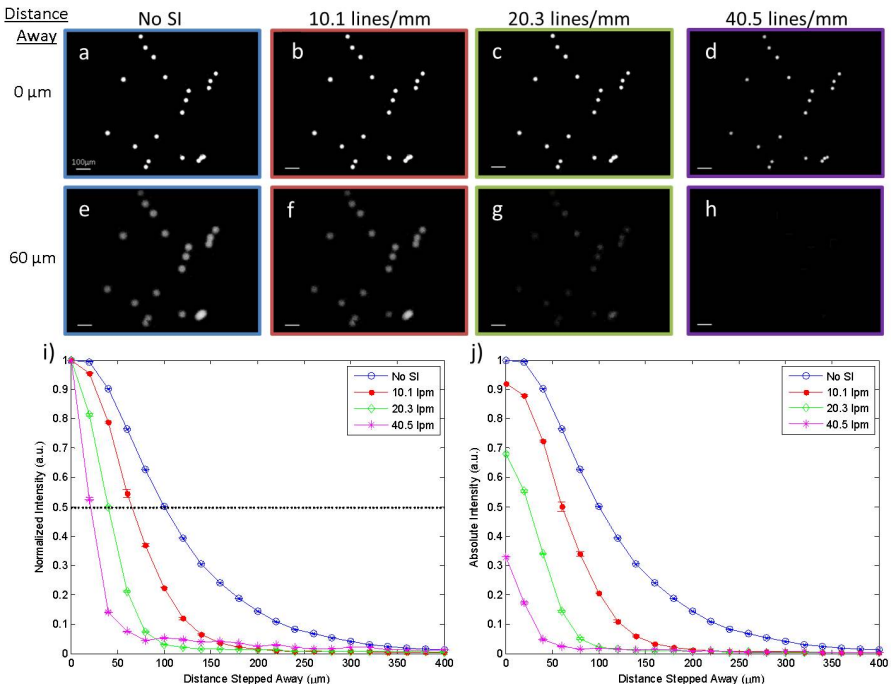

Fig. 2. HRME images of microspheres when the bundle tip was in contact with the sample slide **(a-d)** and 60 µm away from the bundle **(e-h)**. Quantified sphere intensity normalized **(i)** and absolute **(j)** vs distance from the tip of the fiber-bundle to the sample at each modulation frequency. Brightness is adjusted equally for all images to make dimmer spheres more visible.

Figure 2(i) shows the average normalized intensity of the spheres as a function of the distance the glass slide was stepped away from the fiber-bundle. Sphere mean intensity was reduced to half its initial value by 120 µm during imaging without SI. Mean intensity decreased more rapidly during SI imaging depending on modulation frequency. As expected, the higher the modulation frequency, the more rapidly the intensity attenuated. However, as shown in Fig. 2(j), there is a decrease in average initial intensity as a function of frequency. This loss indicates that some in-focus light is also being sectioned more substantially at higher modulation frequencies. The dark stripe at the highest modulation frequency used (40.5 lpm) is approximately three fiber-cores wide, meaning that the grating is approaching the smallest feature resolvable by the fiber-bundle. This limit causes a progressive loss in contrast between the grating image and the sample as the modulation period approaches the fiber-bundle spacing resulting in loss of in-focus signal.

3.2 3D Phantom imaging

Figure 3 shows results from the 3D optical phantom. Figures 3(a)-3(d) shows a sample FOV taken of the non-scattering gel at different modulation frequencies. Spheres not on the surface of the gel appear dimmer, and the apparent diameter is increased due to defocus. As the modulation frequency increases, spheres at greater depths begin to disappear while those close to the surface remained visible, though diminished in intensity at higher frequencies.

#232001 - $15.00 USD Received 7 Jan 2015; revised 9 Feb 2015; accepted 14 Feb 2015; published 19 Feb 2015

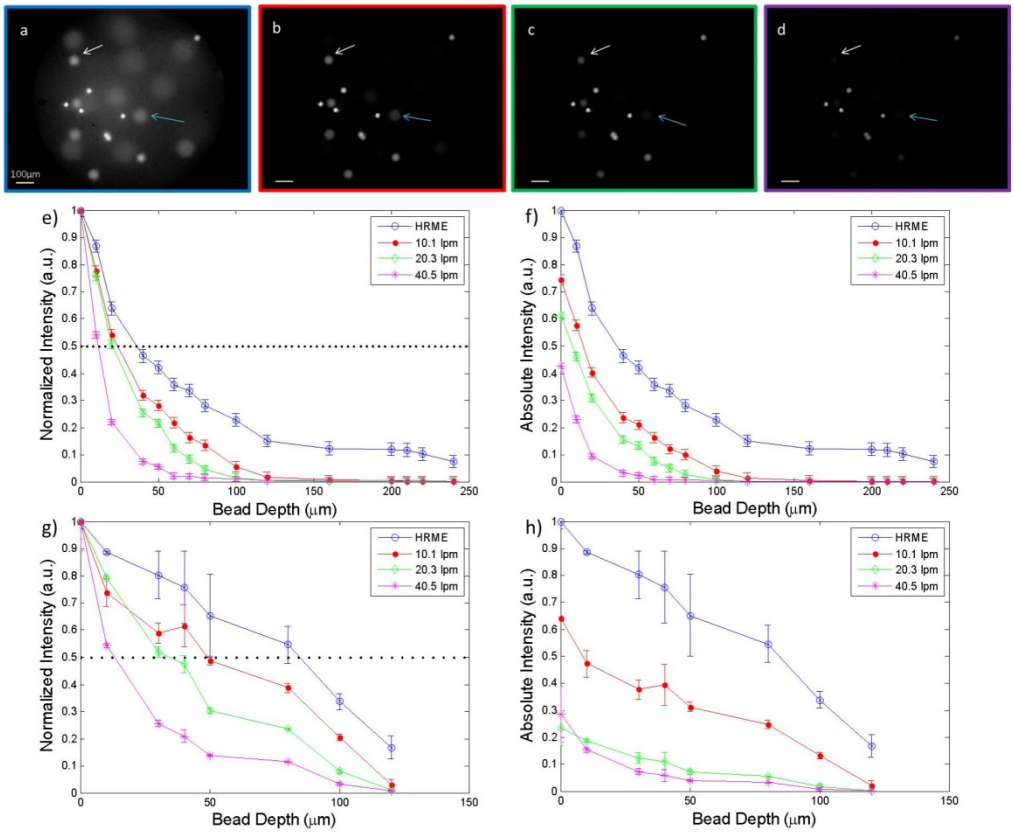

Fig. 3. Sample FOV of the non-scattering gel imaged using HRME with no SI **(a)**, 10.1 lpm modulated SI **(b)**, 20.3 lpm SI **(c)**, 40.5 lpm SI **(d)**. Colored arrows reference spheres which dim significantly at increased modulation frequencies. Sphere intensity normalized **(e)** and absolute **(f)** vs sphere depth in the non-scattering gel. Sphere intensity in the scattering gel normalized **(g)** and absolute **(h)**. Brightness and contrast adjusted equally for all images.

Figure 3(e) quantifies the mean sphere intensity as a function of depth into the non-scattering gel and grating frequency. Again, at higher modulation frequencies mean sphere intensity attenuated more rapidly. Figure 3(f) shows there is also a similar loss in initial intensity as seen in the 2D phantom at higher grating frequencies. A similar pattern is observed in the scattering gel, but the depth at which beads can be seen has been greatly reduced and intensity variation increased (Figs. 3(g) and 3(h)). Multiple fields-of-view from each gel were used to build the graphs shown in Figs. 3(e)-3(h). Spheres in the non-scattering gel at a depth greater than 120 μm, 100 μm, and 60 μm approach zero intensity during SI imaging at modulation frequencies of 10.1 lpm, 20.3 lpm, and 40.5 lpm respectively. Spheres in the scattering gel were too dim to evaluate below 120 μm, and a similar attenuation pattern as seen in the non-scattering gel was observed.

3.3 Ex vivo tissue imaging

Figures 4(a)-4(d) shows HRME images from a region of squamous epithelium on one of the cervical tissue specimens. Individual nuclei are clearly visible in each image; however, the NBRs as shown in Fig. 4(e) increase with higher sectioning strength meaning there is a stronger contrast between nuclear regions and the surrounding background with increased modulation frequency. The standard deviation in the NBRs is the result of propagated error of the nuclear signal and background signal (Fig. 4(f)). Brightness and contrast in Figs. 4(a)-4(d)

#232001 - $15.00 USD Received 7 Jan 2015; revised 9 Feb 2015; accepted 14 Feb 2015; published 19 Feb 2015

were increased to reveal darkened features. However, all NBR values were calculated prior to adjustment.

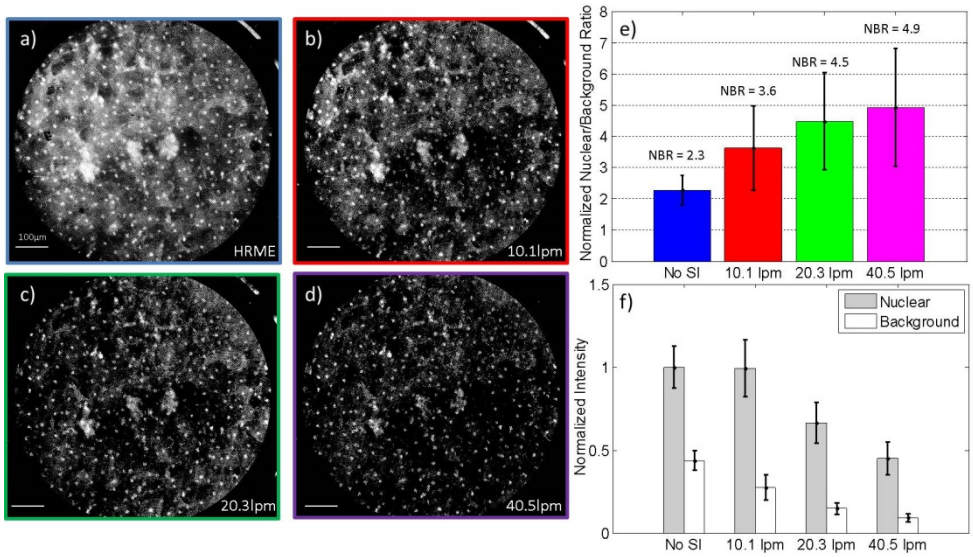

Fig. 4. Squamous epithelium from a cervical tissue specimen. HRME image without SI of the site **(a)**. SI imaging at 10.1 lpm modulation **(b)**, 20.3 lpm **(c)**, and 40.5 lpm **(d)**. Bar graph comparing NBRs for each image (a-d) **(e)**. Nuclear and background signal at each modulation used to calculate the NBRs **(f)**.

Figure 5 shows images at each modulation frequency from different regions of columnar epithelium and illustrates the heterogeneous nature of columnar tissue. In the no SI image at site 1 (Fig. 5(a)) individual nuclei are difficult to observe and overall contrast is visibly poor, but there is a dramatic improvement in contrast after applying SI at 10.1 lpm modulation (Fig. 5(b)). Subsequent higher frequency modulations appear only to darken the image and reduce contrast (Fig. 5(c) and 5(d)). This pattern was also seen in the measured NBRs for site 1 in Fig. 6(a). A large increase in NBR is observed between no SI and 10.1 lpm, but diminishes as the modulation frequency increases.

#232001 - $15.00 USD Received 7 Jan 2015; revised 9 Feb 2015; accepted 14 Feb 2015; published 19 Feb 2015

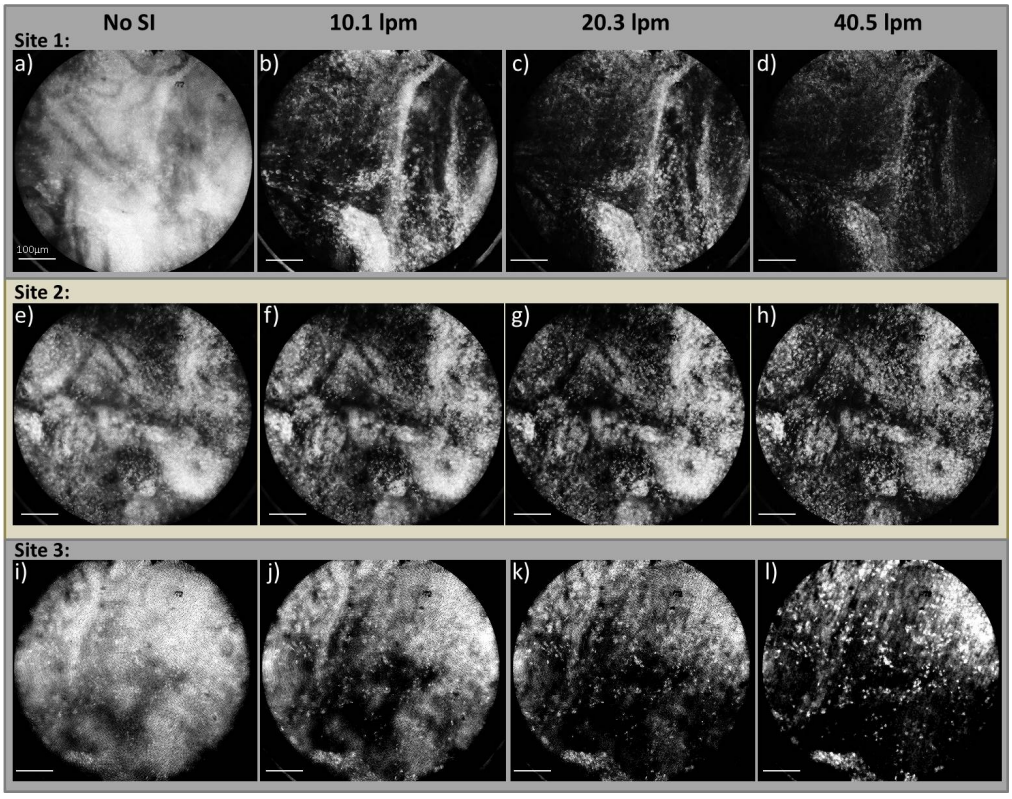

Fig. 5. Images of three sites of columnar epithelium vs SI modulation frequency. Site 1 imaged without SI **(a)**, 10.1 lpm SI **(b)**, 20.3 lpm SI **(c)**, and 40.5 lpm SI **(d)**. Site 2 images **(e-h)**. Site 3 images **(i-l)**. Nuclear morphology becomes more visible with the addition of SI at each site.

At site 2 (Figs. 5(e)-5(h)) the background is reduced incrementally with increasing modulation frequency which reveals previously obscured individual nuclei. The region of densely crowded nuclei on the right side of image showed little visible change in contrast until 40.5 lpm sectioning (Fig. 5(h)). The measured NBR for site 2 incrementally increased with the highest contrast being achieved at 40.5 lpm as shown in Fig. 6(b). At site 3 (Figs. 5(i)-5(l)) individual nuclei are difficult to discern in the no SI image, but become increasingly more visible as modulation is increased. An area of background is first visibly reduced in the lower left quadrant as seen in Fig. 5(j). More background is progressively sectioned away as modulation frequency is increased (Figs. 5(k) and 5(l)). The NBR also correspondingly increases with modulation and is highest at 40.5 lpm Fig. 6(c).

#232001 - $15.00 USD Received 7 Jan 2015; revised 9 Feb 2015; accepted 14 Feb 2015; published 19 Feb 2015

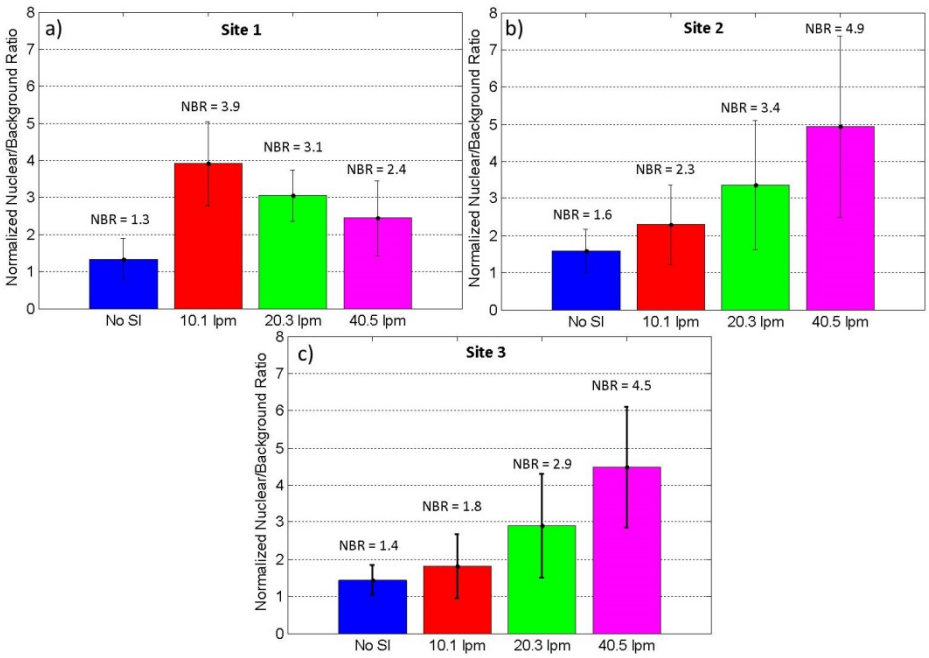

Fig. 6. Nuclear to background ratios of each site shown in Fig. 5. Site 1 NBR increase between the no SI case and 10.1 lpm modulation, but steadily decreases as modulation further increases **(a)**. Site 2 **(b)** and Site 3 **(c)** NBRs steadily increase with modulation frequency.

4. Discussion and conclusion

A portable high resolution microendoscope capable of performing structured illumination in real-time was developed. Results obtained from the phantoms show that the addition of SI attenuates out-of-focus light to a greater extent than light from the focal depth. Thus, the phantoms show that the system can improve image contrast. However, signal intensity is compromised when the period of the modulation frequency approaches the fiber spacing in the bundle. This led us to believe there will be tradeoffs between in-focus signal strength and background removal when translating to tissue. The SI-HRME system then enabled imaging of nuclear morphometry in highly scattering columnar epithelium of the cervix without compromising the ability to image squamous epithelium. However, due to in-focus signal loss, the higher modulation frequencies did not always produce the best contrast. This suggests there must be a balance between sectioning strength and signal loss for optimum contrast in tissue. Future studies will be used to evaluate how the addition of SI affects the detection rate of cervical cancer, assess the ability of the SI-HRME to differentiate different stages of the disease, and to further improve the device.

Structured illumination requires three images to be taken in sequence in order to form one sectioned image, reducing the system's frame rate by three fold. Any motion on the order of microns between these images creates artifacts that can greatly distort the final image. These artifacts were not an issue for our *ex vivo* study where the tissue was not moving relative to the fiber-bundle. However, motion will likely be an issue *in vivo*. High speed systems have been developed utilizing digital-micro-mirrors (DMD) which can greatly increase the frame rate, thus alleviating artifact issues [20]. Furthermore, DMD systems are capable of changing modulation frequency rapidly and could be used to optimize sectioning in real-time since our study found optimal contrast in columnar tissue to be site dependent. However, DMDs often have highly inefficient light transmission [21]. This inefficiency combined with the limits in fluorescent intensity of certain contrast agents, such as proflavine, means that DMD systems

#232001 - $15.00 USD Received 7 Jan 2015; revised 9 Feb 2015; accepted 14 Feb 2015; published 19 Feb 2015

may lack the necessary illumination intensity to image tissue *in vivo* through a fiber-bundle successfully. Future work will require developing a system which can balance the power requirements needed for successful safe *in vivo* imaging, alleviate imaging artifacts, and perform variable amounts of sectioning in real-time. If successful, this system could give clinicians a highly adaptable system capable of imaging tissue architecture in a variety of locations *in vivo*, in real-time, and at the point-of-care.

Acknowledgments

Research reported in this publication was supported by the National Cancer Institute of the National Institutes of Health under Award Number R01CA140257. The authors would also like to thank Dr. Jennifer Carns for her guidance as well as Cindy Melendez and Jessica Gallegos for their assistance with the tissue study. The content is solely the responsibility of the authors and does not necessarily represent the official views of the National Institutes of Health.